POWER MANAGEMENT STRATEGY FOR A GRID CONNECTED WIND/PV/HYDRO/BATTERY/ HYBRID SYSTEM

[1]S.ChandraShekar, [2]Dr. K. Shiva Rama Krishna, [3]P. Venubabu
[1]PG Student, [2,3]Assistant Professor
[1,2,3]Department of Electrical and Electronics Engineering
[1,2,3]J.B.Institute of Engineering and Technology, Hyderabad.

Abstract: This work deals with the frequency regulation, voltage regulation, power management and load levelling of solar photovoltaic (PV)-battery-hydro-wind based micro grid (MG). In this MG, the battery capacity is reduced as compared to a system, where the battery is directly connected to the DC bus of the voltage source converter (VSC). A bidirectional DC–DC converter connects the battery to the DC bus and it controls the charging and discharging current of the battery. It also regulates the DC bus voltage of VSC, frequency and voltage of MG. The proposed system manages the power flow of different sources like wind and hydro and solar PV array. However, the load levelling is managed through the battery and wind. The battery with VSC absorbs the sudden load changes, resulting in rapid regulation of DC link voltage, frequency and voltage of MG. Therefore, the system voltage and frequency regulation allows the active power balance along with the auxiliary services such as reactive power support, source current harmonics mitigation and voltage harmonics reduction at the point of common interconnection. Advanced power technologies are being introduced to improve the characteristics of the wind turbines, and make them more suitable for integration into the power grid. Mathematical model of DFIG with current control loop using PI controller is designed to maximize the power extracted from the wind. Simulation results In MATLAB/SIMULINK show the effectiveness of the strategy Proposed.

***Index Terms* - Pv system -wind system-pi controller- power grid-VSC-hydro system-battery** system-**converters-active power-turbine.**

1. INTRODUCTION

In the present scenario, the proliferation of energy demand of households and industries, create challenges and set a limit on the power generation from the conventional energy sources [1]. The solution to this problem lies somewhere in the core of power generation through renewable energy sources (RES) [2], with efficient, cost effective and reliable generation through RES. The rural electrification is provided by a standalone diesel generator and an integration of other RES in However, the setback for this technology is an RES intermittent nature. This leads to the component over sizing while designing any hybrid renewable energy based micro grid (MG). This also increases the initial cost, operational cost, and life cycle cost.

These topologies based MGs are possible at those places, where grid availability is easy. However, the proposed topology is also possible in rural areas. Merabet et al. [10].system have reported the wind, PV and battery based MG. They have established the control algorithm to look after the power compatibility and power management among different RES in the MG. Wind and PV both being of intermittent nature, present a problem to the optimal sizing [of the energy storage. T

The small hydro system up to 100 kW rating does not require governor control based turbine prime mover and curtails down the cost of the turbine. The generator used in the small hydro has many variations. Synchronous generator, permanent magnet synchronous generator, synchronous reluctance generator and self-excited induction generator (SEIG) , are some of them. However, the most cost effective, efficient, rugged, and easy to use generator in the small hydro system is SEIG. Additionally, the maintenance requirement is also less as compared with its synchronous counterpart. Moreover, SEIG has the drawback that it demands reactive power or magnetizing current for producing the desired terminal voltage.

In this system, PV-battery-hydro based MG is designed for low voltage, which supplies power to small pockets of customers. The proposed MG consists of two energy sources namely hydro and PV with BES. The hydro-based MG adds stiffness and inertia to the system voltage and also increases the reliability of the MG as compared with the wind based MG. An integration of BES eliminates the need for a dump load and adds to the functionality of the MG. This BES is controlled by a bidirectional converter, which reduces the capacity of storage and utilizes the battery effectively. Moreover, BES maintains the continuity of the supply in varying load conditions. The proposed MG has the following distinctive features:

(i) In the proposed MG, the hydro generator runs at almost constant power, therefore, the sudden load change causes the frequency and generated a voltage at PCI to vary. One way of regulating the voltage and frequency is by controlling the water inlet to the hydro through the mechanical controller. Therefore, the mechanical speed regulator is not suitable for sudden changing loads. Therefore, in this proposed MG, the storage battery with VSC, is used to regulate the frequency of the system.

(ii) During the period of a load change, the controller estimates the load power demand and total generated power. If the load demand is more than the generated power, the controller draws the remaining power from

the battery to balance the power demand.

(iii) The proposed MG is also suitable to feed the non-linear load and the harmonic currents required by the non-linear load are supplied by the VSC. Therefore, the hydro generator does not supply the harmonic currents and voltage at PCI is of good quality.

(iv) The proposed MG mitigates the negative impacts of solar PV array caused by the intermittent nature of the solar irradiance. Due to this intermittency, the power generated by the solar PV array changes continuously. Therefore, the storage battery absorbs power fluctuations and maintains the frequency of the MG.

(v) In the proposed MG, the battery is connected to the DC link of the VSC through BDDC, rather than connecting the

battery directly at DC link.

\

2. Proposed Wind System

Wind is abundant almost in any part of the world. Its existence in nature caused by uneven heating on the surface of the earth as well as the earth's rotation means that the wind resources will always be available. The conventional ways of generating electricity using nonrenewable resources such as coal, natural gas, oil and so on, have great impacts on the environment as it contributes vast quantities of carbon dioxide to the earth's atmosphere which in turn will cause the temperature of the earth's surface to increase, known as the greenhouse effect. Hence, with the advances in science and technology, ways of generating electricity using renewable energy resources such as the wind are developed. Nowadays, the cost of wind power that is connected to the grid is as cheap as the cost of generating electricity using coal and oil. Thus, the increasing popularity of green electricity means the demand of electricity produced by using nonrenewable energy is also increasedaccordingly.

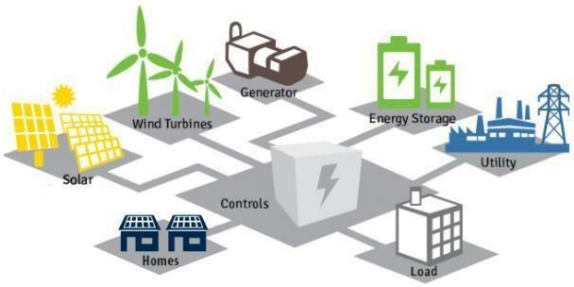

Fig. 1. Renewable energy micro grid

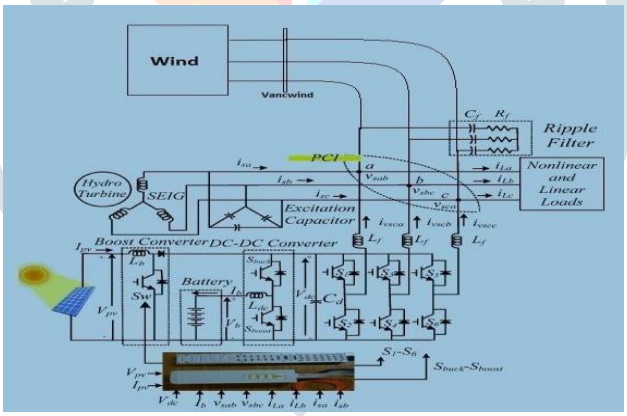

Fig.2 Block diagram Wind power has the following advantages

over the traditional power plants.

- Improving price competitiveness,
- Modular installation,
- Rapid construction,
- Complementary generation,
- Improved system reliability, and
- Non-polluting.

The proposed MG consists of two RES namely hydro, solar PV array along with a BES, a boost converter for MPPT operation and a BDDC for the battery control, A SEIG is used as a hydro generator, which is driven by an unregulated turbine operating in the constant power region. A VSC is connected to the PCI through the coupling inductors. The battery shares the common DC bus of the VSC through the BDDC and solar PV system is also connected to the DC bus of the VSC through the boost converter. Moreover, the ripple filter, linear and non-linear loads are connected to the PCI. The hardware implementation of the proposed MG is done using the digital processor (dSPACE-1103).

3. Battery

The minimum energy that can be stored by the battery is given by:

$$E_b = \frac{E_u}{\eta_b} = 245.56\ Wh/day \quad (1)$$

(Assuming efficiency of battery to be 90%)

Assuming that the working voltage for direct current is 12V, then, the net capacity that the battery can store in Ah/day.

The net capacity of the battery depends on the depth of the discharge of the battery (DDP), and the depth of discharge determines the life cycle of the battery. Deep cycle lead acid battery can store 30% to 80% depth taking an assumption of DDP = 30% then the total commercial capacity of the battery is calculated as:

$$C_b = \frac{}{DDP} = = 68.2Ah \quad (2)$$

This value is correct, if only if there aren't cloudy days. Considering cloudy days, let us assume the battery have energy demand of two days.

$$C_b = 68.2\ Ah\ x\ 2 = 136.42\ Ah \quad (3)$$

Hence, the capacity of the battery is taken as 140Ah. Charge controller

The power output required per household if all appliances are functional at the same time is 101W and the voltage required for the solar home system is usually 12V. So, the charge controller must work at a maximum current.Imax=8.4A

3.1 Analysis of Photovoltaic (PV) Power for the Site

a. Declination angle

The declination is the angular position of the sun at solar noon, with respect to the plane of the equator. As the sun tracks beyond and below the equator depending of the time of the year the declination angle is dependent on the day of the year as shown below. Its value in degrees is given by Cooper's equation [4]:

$$= 23.45 \sin\left(\frac{360}{365}(284 + N)\right) \quad (4)$$

Where N is the day of the year from January 1.

b. Solar hour angle and sunset hour angle

The solar hour angle is the angular displacement of the sun east or west of the local meridian; morning negative, afternoon positive. The solar hour angle is equal to zero at solar noon and varies by 15 degrees per hour from solar noon.

The sunset hour angle ω_s is the solar hour angle corresponding to the time when the sun sets and it is given by

$$\cos \omega_s = -\tan \emptyset \tan \delta \quad (5)$$

Where $\emptyset$ is the latitude of the place.

The solar hour angel is important for calculating the average day light hours using the equation:

$$Ns = \frac{2}{15} cos^{-1}(-\tan \emptyset \tan \delta) \quad (6)$$

Taking the location of our site 12^0North we come across Average day light hours result that shown in Appendix 2. Summarizing the results for each month the trend is depicted in the following figure.3

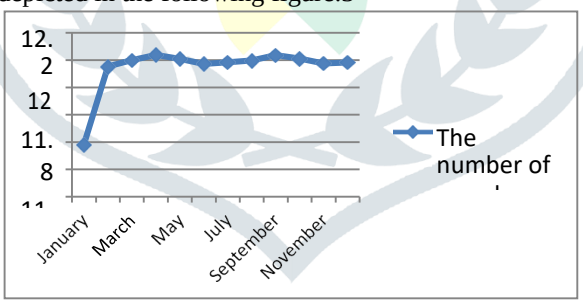

Figure 3 Average day light hours

Average daylight hour depend on the altitude of the site as well as the seasonal orientation of the sun. During January it is known in this area the day length is short being called " Yegena Junber". But since the measured sun shine hours is long there will be a balance between these counters.

C. Extraterrestrial radiation and clearness index

Solar radiation outside the earth's atmosphere is called extraterrestrial radiation. Daily extraterrestrial radiation on a horizontal surface is given by:

$$H_o = \frac{24}{\pi} G_{sc} \left[1 + 0.033 \cos\left(\frac{360N}{365}\right)\right] x \left[\cos \emptyset \cos \delta \sin \omega_s + \frac{\pi}{180} \omega_s \sin \delta \sin \emptyset\right] \quad (7)$$

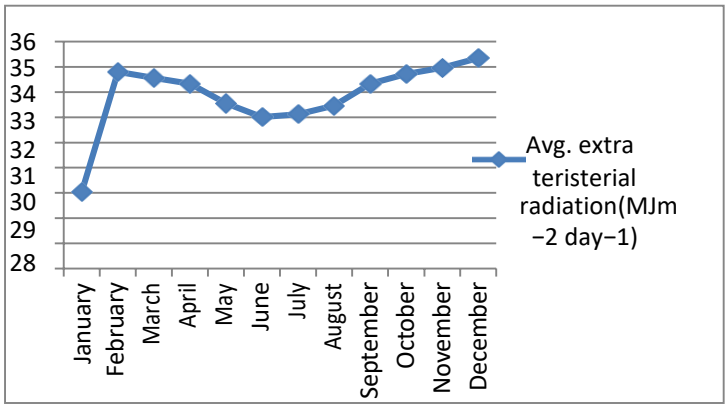

Figure 4 Average extraterrestrial radiation

d. Calculation of average efficiency of PV module

The array is characterized by its average efficiency, $\eta_p$which is a function of average module temperature Tc.

$$= \eta\,(1 - (T_c - T_r)) \quad (8)$$

The average module temperature (Tc) can be obtained from the mean monthly ambient temperature (Ta) through Evans' formula.

$$T_c - T_a = \frac{(219 + 832K)}{800} \quad (9)$$

This Equation is valid when the array's tilt is optimal which is latitude minus declination. If the angle differs from the optimum, the right side of this equation has to be multiplied by a correction factor Cf defined by:

$$C_f = 1 - 1.17x10^{-4}(Z_m - \beta)^2 \quad (10)$$

$$= \emptyset - \delta \quad (11)$$

Energy of the PV array

The power delivered by the PV array (E_p) can be calculated as:

$$= A_p \eta_p \bar{H}_t \quad (12)$$

The array energy available to the load and the battery (E_A) can be obtained by the following relations:

$$E_A = (1 - \lambda_p)(1 - \lambda_c) \quad (13)$$

λ_pMiscellaneous loss like dust cover on the PV array commonly taken as 4%.

λ_c Power conditioning losses commonly taken as 10% The overall array efficiency is defined as:

$$\eta_p = \frac{E_A}{A_p \bar{H}_t} \quad (14)$$

The off-grid model of the PV Array represents stand-alone systems with a battery backup, with or without an additional power generation. Energy from the PV array is either used directly by the load, or goes through the battery before being delivered to the load

4. Micro Hydro Power Generation

Micro-hydro power generation is a very site-specific technology and scheme configurations that varies from site to site. The flow of water in a river may be regulated by means of a small dam or weir. The weir also slightly raises the water level of the river and diverts sufficient water into the conveyance system. The water is channeled to a fore bay tank where it is stored until required and it forms the connection between the channel and the penstock. The penstock carries the water under pressure from fore bay to the turbine. The penstock is a very important part of a hydro project as it can affect the overall cost and capacity of a scheme. The penstock connects to the hydraulic turbine, which is located within the powerhouse.

a. Turbine Selection

A turbine converts energy in the form of falling water in a rotating shaft power. The selection of best turbine for a particular micro hydro site depends on the site characteristics, the dominant factor is the head available and the power required. Selection also depends on the speed at which it is desired to run the generator or other devices loading the generator. From table (1), a turbine type suitable for this site is impulse turbine typically cross flow type.

Table 1. Classification of micro hydro turbines

Classification	TurbineName	Head Range (m)	Flow Range (m^3/s)	Power output
Impulse	Pelton	50-1,000	0.2-3	50-15,000
	Turgo	30-200	0.2-5	20-5000
	CrossFlow	2-50	0.01-2	0.1-600
Reaction	Kaplan	3-40	3-20	50-5000
	Propeller	3-40	3-20	50-500
	FrancisRadial-	40-200	1-20	500-15000
	Francis-Mixed-	10-40	0.7-10	100-5000

b. Sizing of Cross Flow Turbine

For sizing of cross flow turbine, the dimension of interest is the runner length (Lrunner), diameter (Drunner) and jet thickness (tjet). Assuming gear ratio 2 and alternator speed 500rpm,

$$D_{runner} = \frac{42\sqrt{H_{net}}}{N_t}$$

Where:-

$$H_{net} = H_g - h_{hydr} \quad H_{hydr} \text{ is usually 2 to7\% of Hg} = H_g - 7\% of H_g = 9.3m$$

Turbine speed (Nt)= $Alternator\ rpm\ gear\ ratio = \frac{500}{2} = 250rpm$

$$Drunner = \frac{41\sqrt{9.3}}{250} = 0.50\text{m}$$

The jet thickness is usually one tenth of the runner diameter

$$t_{jet} = 0.1xD_{runner} = 50mm \quad (16)$$

Having tjet, the approximate runner length (Lrunner) can be obtained from the orifice discharge equation. The runner length will be equivalent to the jet width.

$$Q = A_{nozzle} = t\,xL_{runner}\,x\sqrt{2gH_{net}} \quad (17)$$

For Q=1.284m^3/s (Alwha river)

$$L_{runner} = 1.902\ m$$

C. Turbine efficiency

For this condition, it is assumed that the three parameters design flow(Q_d),flow at anytime(Q) and peak flow(Q_p)be equal.

$$e_t = 0.79 - 0.15\left(\frac{Q_d - Q}{Q_p}\right) - 1.37\left(\frac{Q_d - Q}{Q_p}\right)^{14} \quad (18)$$

Hence, turbine efficiency will be 0.79 or it is possible to read from equ (14) approximately equal to the calculated value.

5. Design of PV boost converter

The solar PV array is made of modules, which are connected in series and parallel. In an experimental prototype, a solar PV array rating is considered as 2.48 kW. The solar PV maximum power is extracted in two stages. The first stage is to harness the maximum available from the solar PV array using a boost converter and the second stage is to deliver the maximum harnessed power to the load and the battery. The input voltage of a boost converter is the maximum power point (MPP) voltage of the PV array, which is considered as 307 V. The inductor (Lb) of the boost converter is designed for a duty cycle estimated as

$$D = Vdc - Vpv / Vdc = 360 - 307 / 360 = 0.147. \quad (19)$$

The designed value of a boost inductor is given as [8]

$$V\ Lb = \Delta mpirp \times\times Dfs = 0.1 \times 3078 \times\times 200.15 \times 103 = 2.87mH \cong 3mH, \quad (20)$$

Where the ripple current is equal to 10% of the solar PV current at MPP and f s is switching frequency, which is considered as 20 KHz.

a. Design of DC bus capacitor and coupling inductors of VSC

The minimum DC bus voltage for power transfer should be at least equal to 1.1 times the peak of line voltage, i.e. Vdc = 1.1 × V sab × 2 = 230 × 2 × 1.1 = 358V. Therefore, a DC bus

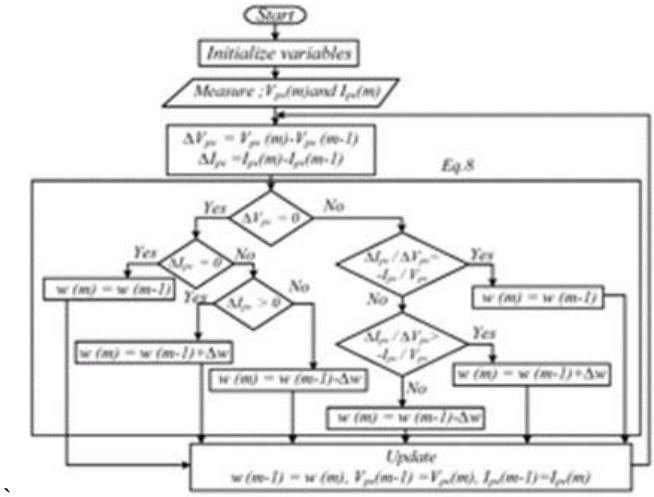

Fig. 5 Micro grid Topology and MPPT Control

(a) Proposed PV-battery-hydro MG, (b) INC based MPP algorithm.

Capacitance is calculated for DC bus voltage of 360 V and it is given as Cd ≅ 3000 μF (21) The interfacing inductor is designed for elimination of high frequency switching harmonics from the VSC current. The coupling inductor is designed as m×Vdc = 360

Lf = 6 × fs ×h× Δic = 6 × 10 × 103 ×1.2 × 11 × 0.10= 4.5 ≅ 5mH. (22)

Where fs is the switching frequency and it is considered as 10 KHz. Δic is the ripple current and it is considered as 10% of fundamental supply current. m and h are the constant values, which are considered as 1 and 1.2, respectively.

b. Design of bidirectional converter

The bidirectional DC–DC inductor (BDDC), which connects the battery to the DC bus, is designed to operate as a buck converter while charging the battery and operates as a boost converter in the battery discharging mode. This inductor of the BES is designed as,

For buck mode operation of the bidirectional converter, filter inductor of the battery is designed as

duty cycle(D) = Vb/Vdc = 240/360 = 0.66, and an inductor, Ldc is as Ldc mH (23)

Where Vb is the battery voltage and it is 240 V, Vdc is the DC-link voltage and it is considered as 360 V. ΔIL is the ripple current and it is considered as 20% of charging current. fs is the switching frequency and its value is 20 kHz.

For boost mode operation of bidirectional converter, the filter inductor of the battery is designed as

duty cycle (D) = (Vdc − Vb) / Vb= (360 − 240)/360 = 0.33Ldc. (24)

Where Vdc is the DC link voltage and it is 360 V. Vb is the battery voltage and it is 240 V. ΔIL is the ripple current and it is considered as 20% of discharging current. Therefore, the filter inductor of the BES is considered as 4 mH.

C. Design of battery and ripple filter

Based on the total capacity of the hydro and solar PV array, the energy storage system capacity is selected. In case, the load is isolated from the MG, the battery shod be able to take the whole generated power of the hydro and solar PV array. Moreover, in this extreme operating condition, the battery should regulate the frequency and voltage of the MG. Hence, the battery rating is selected as 240 V, 14 Ah. The ripple filter is designed to suppress the high-frequency noise caused by the switching the VSC. The ripple filter is a low pass filter and it is the series combination of the capacitor and resistance and their values, are selected as 10
μF and 5 Ω. The other parameters of the MG are given in the Appendix.

6. CONTROL STRATEGY

The details of the control algorithm are given here, which are used for maintaining frequency and voltage of the system. Here, an INC-MPPT technique harnesses the maximum power from the solar PV array and the battery is controlled by a bidirectional controller.

a. INC-based MPP strategy

The proposed MG consists of two renewable energy systems one is hydro and another one is solar PV system as shown in Fig. 1*a*. The maximum power of the solar PV array is extracted in two stages. One stage is the MPP algorithm, which estimates the duty cycle of a boost converter for achieving maximum power. The second stage is the VSC, which delivers a maximum power of the PV system to the battery and the load. The INC-based MPP technique is used for harnessing the maximum power from the PV system as shown in Fig. 1*b*. The maximum available power is given as,

$$P_{mpp} = V_{pv} \times I_{pv} . \quad (25)$$

The MPP point is achieved at that point where the PV power derivative with respect to the PV voltage is equal to zero. The governed equations of INC algorithm is given as

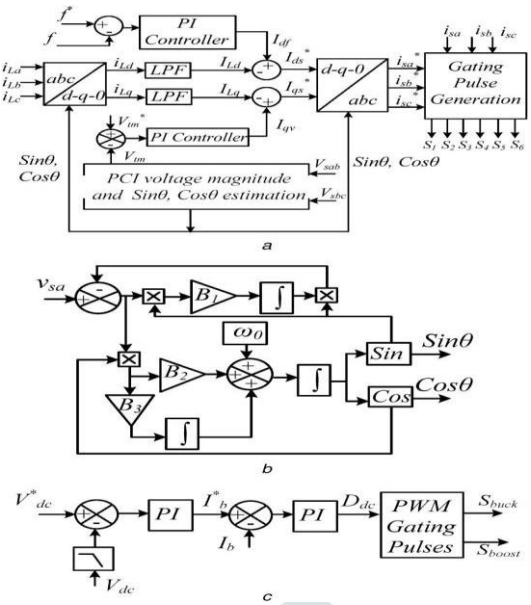

Fig. 6 Control *diagram of standalone MG*

(a) Control algorithm for VSC, *(b)* Estimation of sin θ and cos θ components, *(c)* Controller for BDDC

if $\Delta I_{pv}/\Delta V_{pv} > -\Delta I_{pv}/\Delta V_{pv}$, then $\omega(m) = \omega(m-1) + \Delta\omega$,

if $\Delta I_{pv}/\Delta V_{pv} = \Delta I_{pv}/\Delta V_{pv}$, then $\omega(m) = \omega(m-1) + \Delta\omega$, (26) if $\Delta I_{pv}/\Delta V_{pv} < -\Delta I_{pv}/\Delta V_{pv}$, then $\omega(m) = \omega(m-1) + \Delta\omega$,

where I_{pv} and V_{pv} are the sampled PV current and PV voltage of the array, $w(m)$, $w(m-1)$ and Δw are the estimated, old and change in the duty ratio.

signal. Therefore, EPLL reduces the computational burden of DSP (dSPACE-1103) and the dynamic response is fast for estimation of phase and frequency. The schematic diagram of EPLL is shown in Fig.6. The EPLL constants, B_1, B_2, and B_3, are selected as per the procedure given.

b. Control strategy for BDDC

The control of the BDDC is shown in Fig. 2*c*. The BDDC regulates the DC bus voltage of the VSC while performing buck or boost operation depending on the battery charging or discharging. Moreover, the control scheme synchronizes the power generation and load demand by storing the surplus power into the battery. Similarly, the deficit power is supplied by the battery in case the generation is less than the load demand. The DC bus voltage is maintained by a proportional integral (PI) controller, which is expressed as

$I_b^*(k) = I_b^*(k-1) + k_{pvi}\{V_{dcer}(k) - V_{dcer}(k-1)\} + k_{pvp}/V_{dcer}$, (27) Where k_{pvi} and k_{pvp} are the gains of the PI controller, respectively

$V_{dcer}(k) = V_{dc}^*(k-1) - V_{dc}(k)$. (28)

The duty cycle of the converter is governed by a battery current PI controller and it is estimated as

$Ddc(k) = Ddc(k-1) + k_{pii}\{I_{ber}(k) - I_{ber}(k-1)\} + k_{pip}I_{ber}$, (29) Where k_{pii} and k_{pip} are the gains of the PI controller, respectively

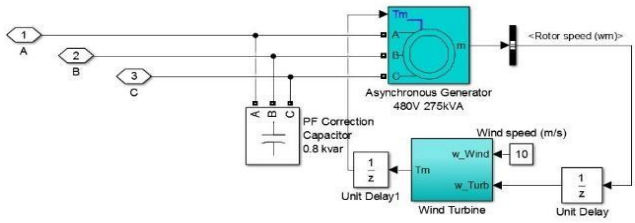

Fig7.Control diagram of wind turbine

7. RESULTS AND DISCUSSION

The proposed MG is implemented for a 3.7 kW hydro based induction generator, PV array simulator and BES. The performance of the proposed system is shown in Figs. 3–8 in a real-time experimental environment. The excitation capacitor of the SEIG has been selected by using the per-phase equivalent model of SEIG as per the procedure given in. The per phase excitation capacitor of 3.7 kW, 230 V, 50 Hz, induction machine is selected as 80 µF/phase. Moreover, these capacitors are connected in delta configuration and it is connected to the generator terminals to maintain the rated voltage. A variable frequency drive controlled induction motor is used for emulating the hydro prime mover. A non-linear load is realised by using the diode bridge rectifier with the R–L load. Six Hall-effect current sensors are used for sensing the source currents (isa and isb), load currents (iLa and iLb), solar PV current (Ipv) and battery current (Ib). Four Hall-Effect voltage sensors are used for

sensing the common point voltages (vsab and vsbc), PV voltage (Vpv) and the DC bus voltage of the converter (Vdc). A PV array simulator (Terra SAS PV) is used to realise a 2.48 kW solar PV, whose maximum voltage (Vmpp) and current (Impp) rating are 307.0 V and 8.0 A, respectively. The control algorithm of the VSC and a bidirectional converter for voltage, frequency and power management, are implemented on a digital controller (dSPACE-1103). The system voltage and frequency regulation are achieved by PI controllers. The PI controllers of the proposed MG are tuned using the Ziegler Nichols step response technique . The detailed values of system parameters are given in the Appendix.

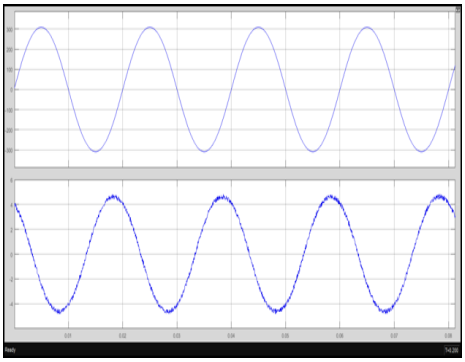

(a)

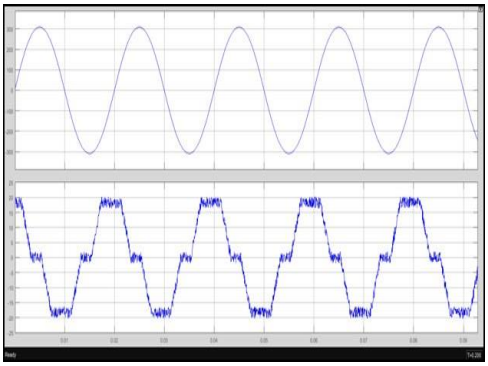

(b)

Fig. 8 *Steady-state performance of PV-battery-hydro system under non-linear load*

(a) PCI line voltage (*v*sab) and source current of phase 'c' (*i*sc), , ***(c)*** *v*sab and *i*Lc*v*sab *and i*vscc,

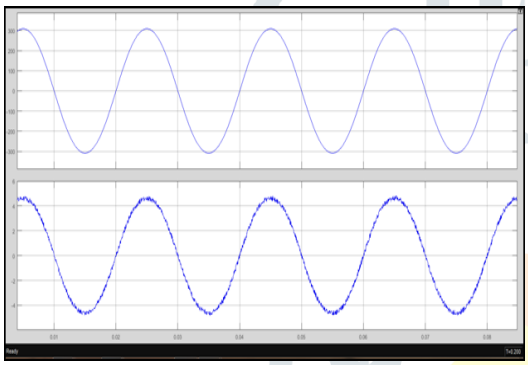

(a)

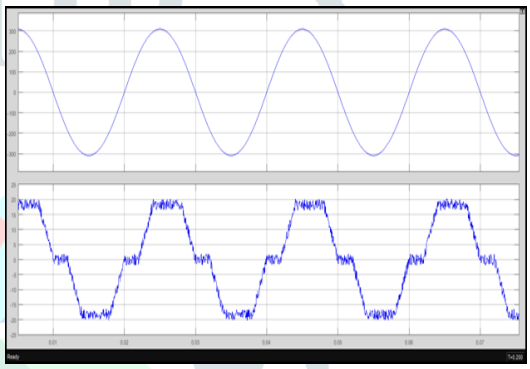

(b)

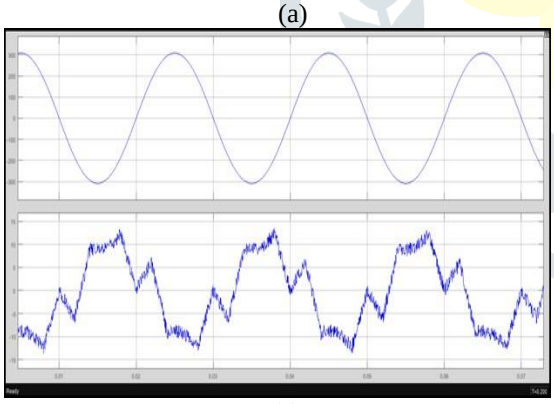

(c)

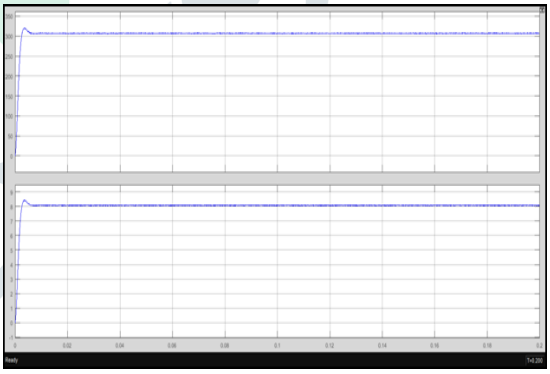

(d)

Fig. 9 *Steady-state performance of PV-battery-hydro system under non-linear load*

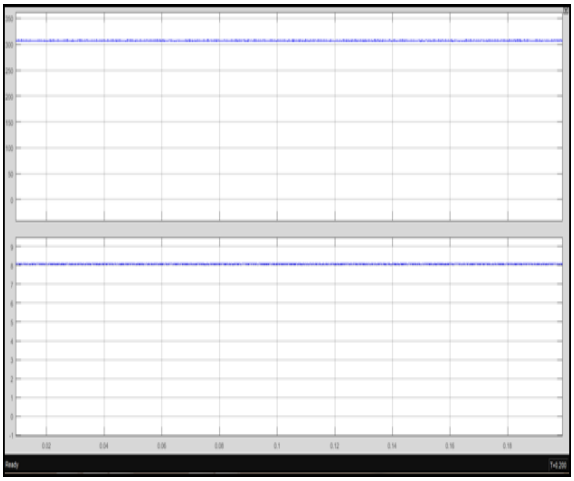

(a)

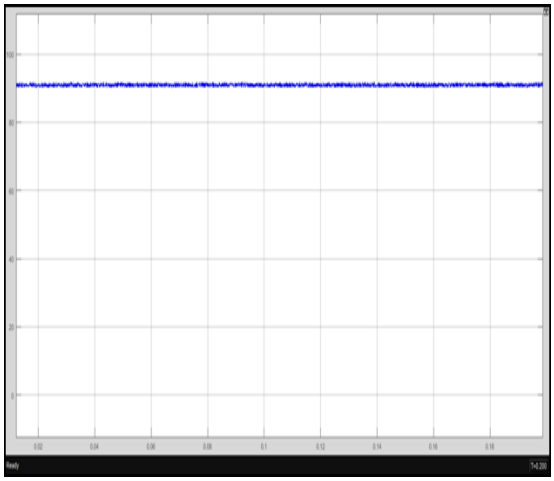

(b)

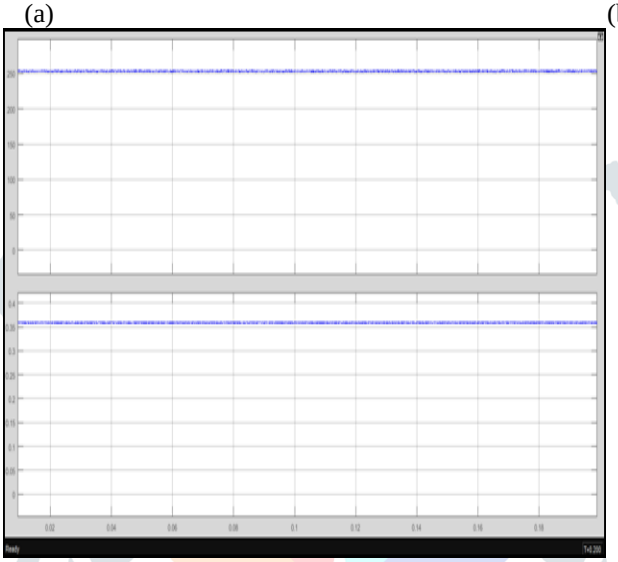

(c)

Fig. 10 Steady-state performance of PV-battery-hydro system under non-linear load (a) Vpv and Ipv, (b) Pb, (c) Vb and Ib,

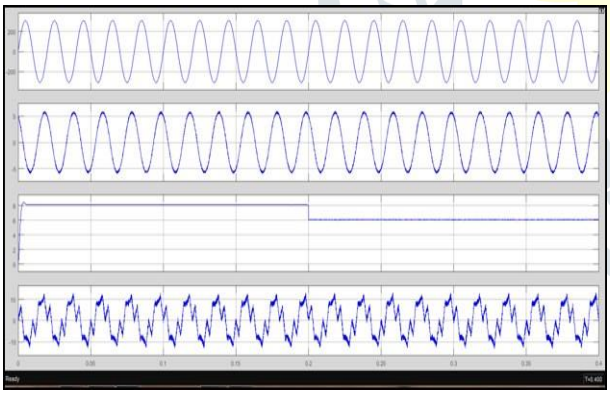

(a)

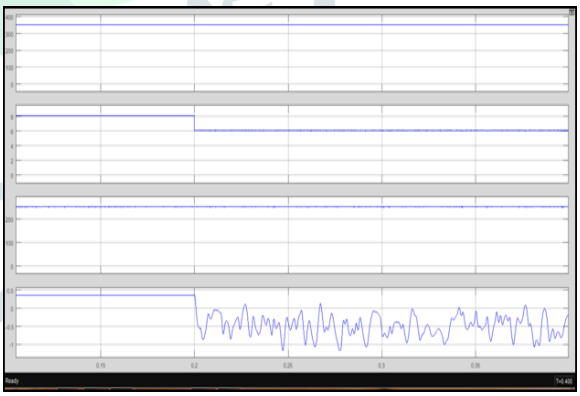

(b)

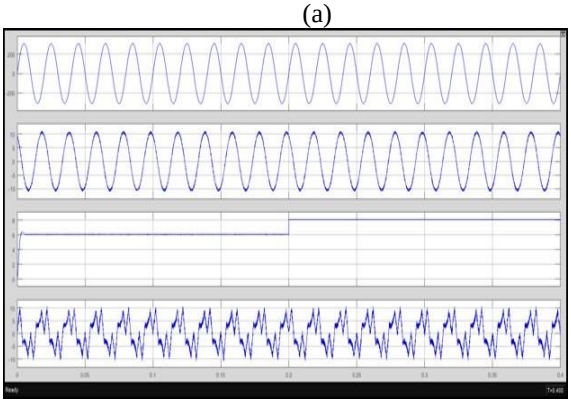

(C)

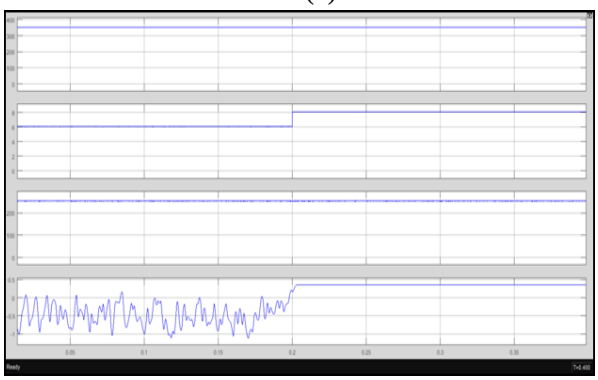

(d)

Fig. 11 Dynamic performance of PV-battery-hydro based MG following by solar irradiance change (a) vsab, isc, iLc and ivscc, (b) Vdc, Ipv, Vb and Ib, (c) vsab, isa, iLa and ivsca, (d) Vdc, Ipv, Vb and Ib

a. Steady-state performance of PV-battery-hydro based MG under non-linear load

The current drawn by the non-linear load contains the harmonics and in the proposed MG, the hydro generated source currents are sinusoidal even when the load currents are non-sinusoidal as shown in Figs. 3a–d. The load is fed through two energy sources, one is hydro and second is PV array as shown in Figs. 4a–d. In the proposed MG, the MPPT algorithm harnesses the maximum available power from the solar PV array and the performance of the MPPT algorithm of the solar PV array simulator in the experimental prototype is shown in Fig. 6a. Solar PV generated power, voltage, and current under maximum power condition and also battery voltage, current and power are shown in Fig. 4d and 5a–c. From Fig. 4d, it is seen that the solar PV generated power is 2.48 kW, which is distributed into three parts (i) supplying the remaining power required by the load, (ii) storing the surplu

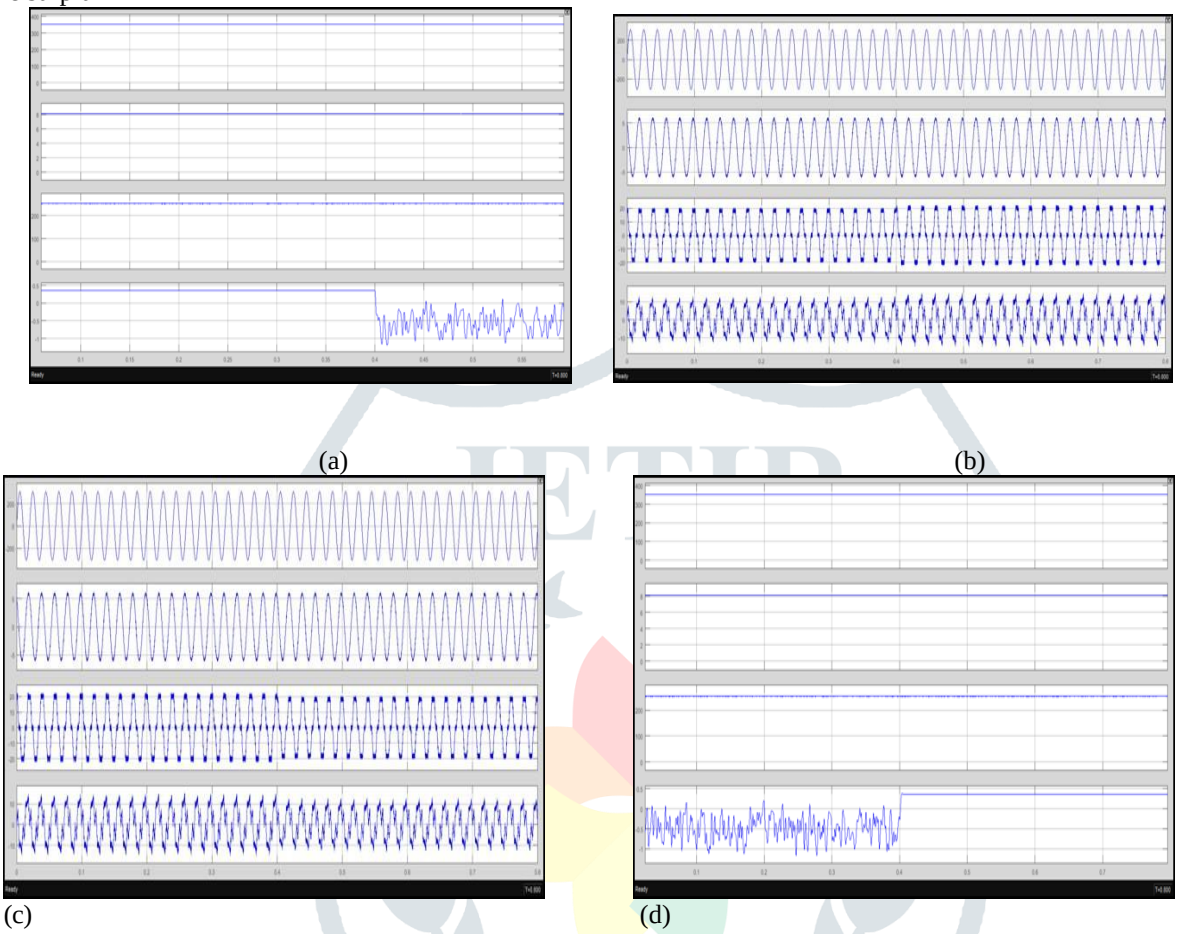

Fig. 12 Dynamic performance of hydro-battery-PV based MG under load perturbation (a) vsab, isc, Ipv and ivscc, (b) Vdc, Ipv, Vb and Ib, (c) vsab, isc, Ipv and ivscc, (d) Vdc, Ipv, and Vb

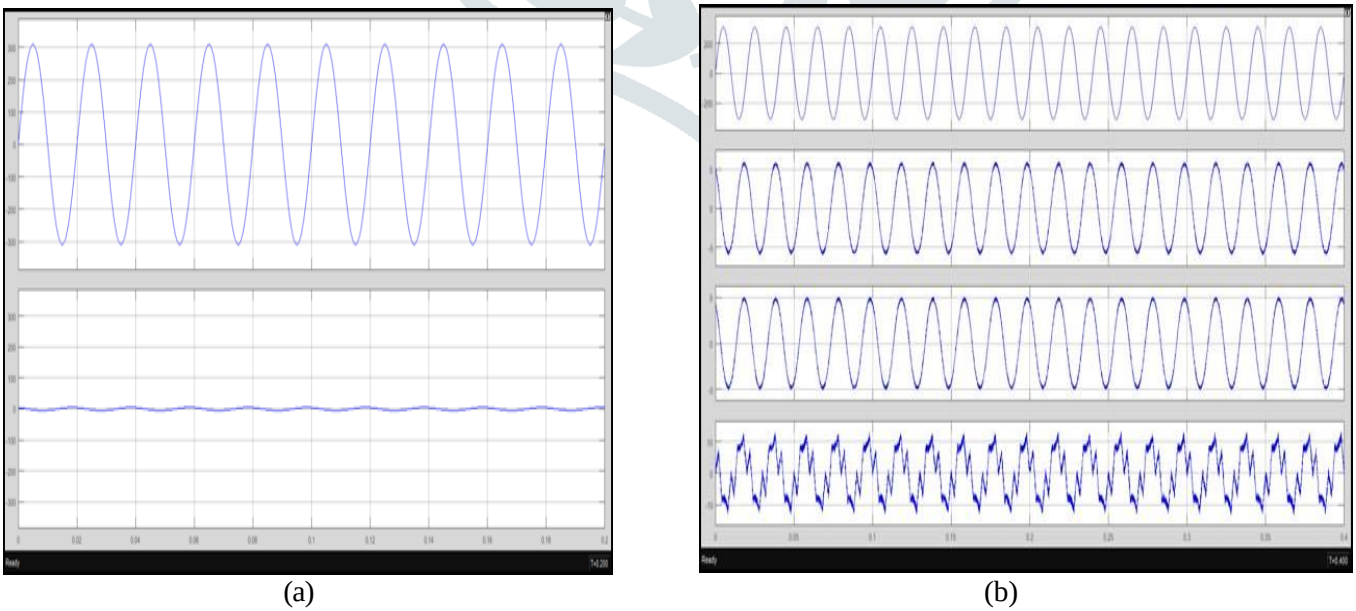

Fig.13 Performance of Wind (a) $Vwind_{abc}$ and $Iwind_{abc}$ (b) VSabc , ISabc , Iwindabc , IVSabc

power in the battery, and (iii) compensating losses of the system. The harmonic spectra of PCI line voltages, source current and load current, are shown in Figs. 3b, d, and 5d. The source current is sinusoidal and its total harmonic distortion

(THD) is 4.1% and source voltage THD is 0.8%, which are well within an IEEE-519 standard. However, the load current THD is obtained as 22.3%.

b. Dynamic performance of PV-battery-hydro based MG under change in solar irradiance

The dynamic performance of the PV-battery-hydro based MG under solar irradiance disturbance is shown in Figs. 7a–d and 6b In Figs. 7a–d, the dynamic behaviour of the PCI voltage (vsab), source current (isc), load current (iLc), VSC current (ivscc), DC-link voltage (Vdc), solar PV array current (Ipv), battery voltage (Vb) and battery current (Ib), is exhibited. Despite the change in solar PV irradiance from 1000 to 790 W/m2, MPP is achieved as shown in Fig. 6b. A reduction in solar PV irradiance, causes the change in solar generated power and consequently, the change in battery operating mode from charging to discharging mode, to meet the load demand as shown in Fig. 7b. The other system parameters remain unaffected and the system remains stable. Similarly, an increase in solar PV irradiance, increases the power generated by the solar PV array. To manage the increased power, the battery changes the operating from discharging to charging as shown in Figs. 7c–d. The DC-link voltage remains unaffected under the solar irradiance disturbances.

C. Dynamic performance of PV-battery-hydro based MG under load perturbation

Fig. 12 presents the dynamic performance of PV-battery-hydro based MG under varying load conditions. Figs. 8a–d show the transient behaviour of the PCI voltage (vsab), source current (isc), load current (iLc), VSC current (ivscc), DC-link (Vdc), solar array current (Ipv), battery voltage (Vb) and battery current (Ib). When the load is increased, load demand exceeds the hydro generated power, since SEIG operates in constant power mode. In this condition, the solar power is diverted to meet the load demand and the battery starts discharging as shown in Figs. 8a and b. Similar is the condition for a decrease in load demand and the battery comes into charging mode, which is depicted in Figs. 8c and d.

The study has covered increase in voltage and power with three renewable sources. System feasibility was designed in terms of economical points was analyzed. The results are indicating:

8. Conclusion:

In this paper, a brief review of wind energy systems is presented mainly focusing on electrical technologies. The most common configurations for the wind energy conversion system (WECS) along with possible future research direction are discussed. Importance of smart wind electrical system is highlighted. In coming time, huge challenging task for wind energy system will be its cost– effectiveness and reliability. Research should be focused to reduce the size and weight of wind turbine to minimize its space requirement. Mostly electric power from wind is sent to grid. But due to erratic nature of wind flow, it is great challenge to comply with grid. This work is intended to present the current technology related to wind electrical system and future research direction. The results from this work are indicating that Wind potential is more promising than solar energy. Solar energy and battery is not attractive due to relatively larger initial investment cost and

Producing locally imported equipment could further reduce the cost that has been previously explored and make further maximized feasibility of the potential sources

9. Future works:

In this, Due to usage of PI controller some loss incurred at output/load side, to eradicate the loss we can use ANN for future expansion and thus approximate values with less tolerance can be acheived.

Appendix

Parameters for proposed MG: 3.7 kW, 230 V, 50 Hz, starconnected and four-pole SEIG, $L_b = 6$ mH, $L_f = 5$ mH; battery capacity 240 V, 14 Ah, EPLL constant $B_1 = 0.1 \times 10^3$, $B_2 = 0.05 \times 10^2$ and $B_3 = 0.02 \times 10^3$; PCI voltage PI controller gain: $k_{pa} = 0.1$, $k_{ia} = 1.6$; $L_{dc} = 4$ mH, PI controller gain of DC–DC bidirectional controller: $k_{pvp} = 2$, $k_{pvi} = 0.0001$and $k_{pip} = 3$, $k_{pii} = 0.0001$; $P_{mpp} = 2.48$ kW, $V_{mpp} = 307.35$ V and $I_{mpp} = 8.086$ A. wind turbine synchronous generator=480w, 275kva, pf correcption

capacitor=0.8Kvar,phasetophasevoltage=415(Vrms),mutualinductance=3.5Lm(Pu).statorresistance(Rs)=0.016Pu.statorinductance (Lis)=0.06Pu.rotarresistance(Rr^1)=0.015Pu.rotaor inductance($Lir)^1$=0.06Pu

REFERENCES

[1] Ellabban, O., Abu-Rub, H., Blaabjerg, F.: 'Renewable energy resources: current status, future prospects and technology', *Renew. Sustain. Energy Rev.*, 2014, 39, pp. 748–764

[2] Bull, S.R.: 'Renewable energy today and tomorrow', *Proc. IEEE*, 2001, 89, (8) , pp. 1216–1226

[3] Malik, S.M., Ai, X., Sun, Y., *et al.*: 'Voltage and frequency control strategies of hybrid AC/DC microgrid: a review', *IET Renew. Power Gener.*, 2017, 11, (2) , pp. 303–313

[4] Kusakana, K.: 'Optimal scheduled power flow for distributed photovoltaic/ wind/diesel generators with battery storage system', *IET Renew. Power Gener.*, 2015, 9, (8), pp. 916–924

[5] Askarzadeh, A.: 'Solution for sizing a PV/diesel HPGS for isolated sites', *IET Renew. Power Gener.*, 2017, 11, (1), pp. 143–151

[6] Kant, K., Jain, C., Singh, B.: 'A hybrid diesel-wind-PV based energy generation system with brushless generators', *IEEE Trans. Ind. Inf.*, 2017, 99, pp. 1–1

[7] John, T., Ping Lam, S.: 'Voltage and frequency control during microgrid islanding in a multi-area multi-microgrid system', *IET Gener. Transm. Distrib.*, 2017, 11, (6), pp. 1502–1512

[8] Philip, J., Jain, C., Kant, K., *et al.*: 'Control and implementation of a standalone solar photo-voltaic hybrid system', *IEEE Trans. Ind. Appl.*, 2016, 52, (4), pp. 3472–3479

[9] Kwon, M., Choi, S.: 'Control scheme for autonomous and seamless mode switching of bidirectional DC–DC converters in a DC microgrid', *IEEE Trans. Power Electron.*, 2017, early access

[10] Merabet, A., Tawfique Ahmed, K., Ibrahim, H., *et al.*: 'Energy management and control system for laboratory scale microgrid based wind-PV-battery', *IEEE Trans. Sustain. Energy*, 2017, 8, (1), pp. 145–154.